Meccanica (2005) 40: 163–179
DOI 10.1007/s11012-005-3064-3

Thermal Residual Stresses in Graded Ceramic Composites: A Microscopic Computational Model Versus Homogenized Models

P. VENA*
Dipartimento di Ingegneria Strutturale, Laboratory of Biological Structure Mechanics, Politecnico di Milano, Piazza Leonardo da Vinci, 32, 20133 Milano, Italy

(Received: 14 January 2004; accepted in revised form: 28 January 2005)

Abstract. Thermal residual stresses in ceramic composite laminates are analyzed through both a micromechanical computational model and two macroscopic homogenized models. The microscopic model is based on a purposely developed hybrid finite element able to account for the shape of the Alumina and Zirconia grains. Two different macroscopic models have been used as reference solutions for comparison: a standard displacement-based three-dimensional finite element model and an analytical model. Stress concentration factors, accounting for the microscopic material heterogeneities, have been estimated by means of the Eshelby tensor and applied to the average stress field obtained through the homogenized models.

Key words: Ceramic composites, Layered structures, Micromechanical finite element analysis.

1. Introduction

The extensive use of advanced ceramics in many industrial fields and the advancements in the manufacturing techniques, through which innovative devices are now available, require the development of sophisticated analysis methods. These methods must be able to predict the material behaviour under service loading, that is strongly affected by the manufacturing process.

This paper deals with computational models for the estimation of the residual stress field induced by the cooling process of composite ceramic laminates obtained through sinterization performed at 1600°C.

A symmetric laminate with alumina/zirconia composites having a different volumetric composition in each lamina is considered.

In this kind of structures, the thermal stresses are due to both the mismatch of the mean coefficient of thermal expansion (CTE) between the laminae, and to the CTE mismatch between the alumina and the zirconia grains within each lamina [1, 2].

An accurate estimation of the thermal stress field is mandatory when designing any reliable device. Indeed, delaminations or cracking due to the residual stresses can occur if the thickness of the laminae is larger than a critical value [3] and transverse cracks (channelling) are also possible [1]. Moreover, the thermal residual stresses can increase or decrease the material toughness depending on the stacking sequence.

*Tel.: +39-02-2399 4236; Fax: +39-02-2399-4220; e-mail: vena@stru.polimi.it

The numerical estimation of the residual stress field in composite laminates has been extensively studied at the macroscopic scale. Purposely developed finite element formulations or analytical models able to capture the stress concentrations at the free boundary have been discussed, see for example [4–6]. At the microscopic scale, several papers can be found, focusing on computational and analytical models for heterogeneous materials subjected to a temperature change and aimed at estimating the stress concentration factors in the phases of the material, e.g. [7–9].

In particular, in [10] thermal residual stresses in functionally graded materials are computed through the Voronoi Cell Finite Element model solving a coupled heat conduction-mechanical analysis.

Several works having the purpose of bridging the two length scales – the laminate scale and the microstructure scale – can be found; one example is the one by Schmauder and Weber [11].

Examples of multiple scales analyses based on the homogenization theory with the coupling of microstructural and macroscopic models are discussed in [12] with specific reference to metal matrix composites. Coupling of macroscopic model and Voronoi Cell Finite Element microscopic models are presented in [13].

In this paper a comparison between a micromechanical hybrid finite element model and two different homogenized macroscopic models is discussed. In contrast to the papers based on homogenization theory [13], no coupling between the two length scales is here considered.

A hybrid finite element approach, with stress and displacement interpolation on polygonal domains and based on the formulation proposed by Ghosh and Moorthy in [14], has been adopted for the microstructural modeling of the composite. This finite element approach allows considering the specific geometrical features of the ceramic composite microstructure, which has polygonal shaped alumina and zirconia grains. The accuracy and the computational cost saving of this approach with respect to the standard displacement-based finite element microstructural analysis have been proved Moorthy and Ghosh in [15].

Two different homogenized models have been adopted for the analysis at the macroscopic scale of the laminate: (i) a standard three-dimensional displacement-based finite element formulation and (ii) an analytical model based on an assumed stress distribution and on the minimum complementary energy theorem [16,17]. Provided that the laminate under consideration is symmetric and that each lamina is made of isotropic material, the latter approach turns out to be rather convenient and therefore worth to be used for comparison purposes.

The macroscopic analyses are carried out by considering homogenized material properties of the composites, for the various material compositions, which have been obtained by the Author in a previous research through an homogenization technique [18].

Stress concentrations in the material components within each lamina, owing to the CTE mismatch between alumina and zirconia grains, have been estimated through the Eshelby tensor by assuming as a simplified geometry for the composite representative volume element a spherical inclusion embedded in a spherical matrix.

The outline of the paper is as follows: after a brief description of the mechanical properties of the alumina/zirconia composites reported in Section (2), the computational micromechanical finite element model is expounded in Section (3).

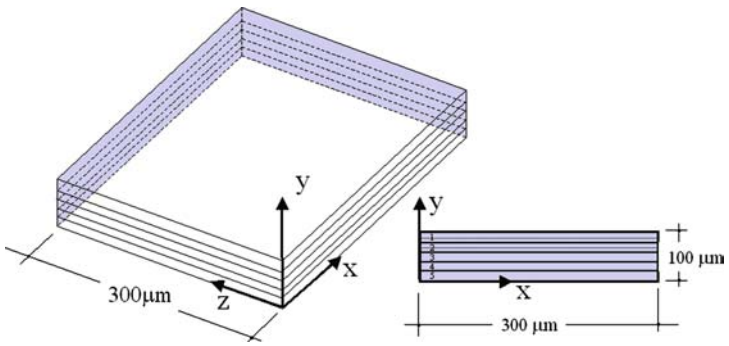

Figure 1. Sketch of one eighth of the laminate and layer numbering; the symmetry transversal planes are shaded.

The macroscopic homogenized models are discussed in the Section (4): the 3D displacement-based finite element model and an analytical model are described in subsections (4.1) and (4.2), respectively.

Section (4.3) reports the Eshelby approximation of the stress concentration factors in the Alumina and Zirconia phases. The results and a critical discussion follow in the last section.

2. The alumina/zirconia Graded Composite

A ten layers symmetric laminate of alumina/zirconia composite has been considered in this paper. Each layer has a uniform thickness of $20\,\mu$m. Different alumina/zirconia volume fractions are assumed in each layer. A sketch of the laminate is reported in Figure 1; due to symmetry, only one eighth of the laminate is reported.

The manufacturing process involves a sinterization of the ceramic powders, performed at 1600°C [19]. The high temperature promotes the powder growth and the process yields a composite material exhibiting a microstructure characterized by polygonal grains of alumina and zirconia, both having an average size of $1\,\mu$m.

A uniform temperature field is assumed throughout the laminate. The temperature drop of $\Delta\theta = -1600$°C is applied to all the points of the model. The transient phase during which the heat flaw causes a temperature gradient within the material has been neglected due to the values of the thermal conductivity of the material and due to the small thickness of the laminate.

Both the alumina and zirconia phases are assumed to be isotropic linear elastic materials. Isotropy of the Coefficient of Thermal Expansion, CTE (α) is also assumed. However, anisotropic CTE often exists in the alumina and zirconia grains depending to the mean orientation of the crystal lattices. The constitutive parameters used in the microscopic model, which accounts separately for the zirconia and alumina phases, are reported in Table 1. The material compositions of the five layers above the symmetry plane of the laminate is reported in Table 2 (layer numbering starts from the outer-most layer).

The macroscopic material properties of the composites in each lamina have been obtained by means of finite element homogenization analyses. The results of the homogenization method are reported by Vena *et al.* [18] and summarized in Figure 2.

Table 1. Parameters of the isotropic linear elastic constitutive model for the alumina and zirconia

	E[GPa]	ν	$\alpha[^{\circ}C^{-1} \times 10^{-5}]$
Alumina	415	0.23	0.775
Zirconia	210	0.29	1.06

Table 2. Stacking sequence of the five laminae above the symmetry plane

Layer N	$\%ZrO_2$	$\%Al_2O_3$
1	100	0
2	80	20
3	60	40
4	40	60
5	20	80

Upper and lower Hashin and Shtrikman bounds are also reported [20]. The homogenization analyses provided the Poisson's ratio and the Young modulus of an equivalent isotropic continuum ν^H, E^H; as well as the coefficient of thermal expansion α^H, for a given zirconia volume content in an alumina matrix. Comparisons with experimental data have been used in order to validate the homogenization numerical results. The constitutive parameters that have been used in the macroscopic models, resulting from the homogenization analyses are reported in Table 3.

3. The Voronoi Cell Finite Element Method (VCFEM): the Basic Formulation

The formulation for the polygonal Voronoi Cell Finite Element is based on the extension of the hybrid finite element formulation, originally introduced by Tong and Pian [21], presented by Ghosh and Mukhopadhyay [22].

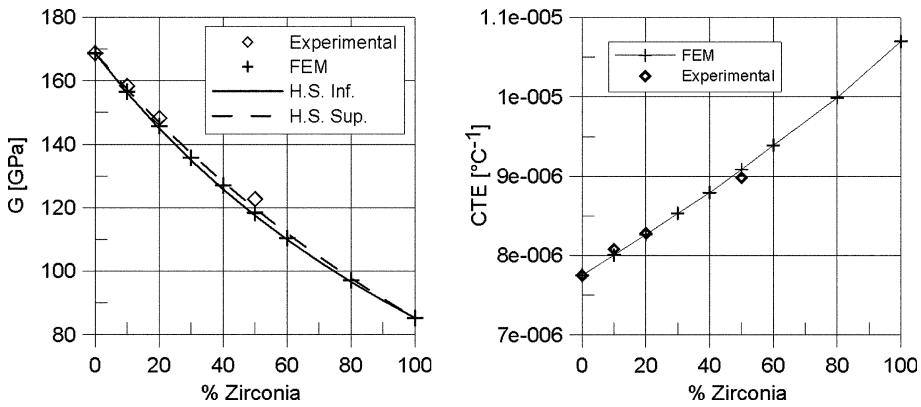

Figure 2. Results of the homogenization analyses of the macroscopic mechanical properties as function of the Zirconia volume content: Elastic tangential modulus (left), coefficient of thermal expansion (right).

Table 3. Parameters of the homogenized linear elastic isotropic constitutive models for the five layers above the symmetry plane

Layer N	E^H[GPa]	ν^H	$\alpha^H[^\circ C^{-1}] \times 10^{-6}$
1	210	0.29	10.57
2	248.561	0.28	9.99
3	280.024	0.269	9.39
4	319.465	0.257	8.79
5	362.608	0.244	8.26

A brief description of the finite element formulation in the plane strain setting is here summarized using the matrix notation.

In plane problems, the stress and strain components, in the plane of the model, are collected in vectors $\boldsymbol{\sigma}$ and $\boldsymbol{\epsilon}$ according to the following notation:

$$\boldsymbol{\sigma} = \begin{bmatrix} \sigma_1 \\ \sigma_2 \\ \tau_{12} \end{bmatrix}; \quad \boldsymbol{\epsilon} = \begin{bmatrix} \epsilon_1 \\ \epsilon_2 \\ \gamma_{12} \end{bmatrix}. \tag{1}$$

The inverse isotropic linear elastic constitutive relation is therefore written as:

$$\boldsymbol{\epsilon} = \mathbf{S}\boldsymbol{\sigma} + \boldsymbol{\theta} \tag{2}$$

in which $\mathbf{S}$ is the elastic compliance matrix of the material. The vector $\boldsymbol{\theta}$ collects the thermal strains that in a plane strain state are:

$$\boldsymbol{\theta} = (1+\nu)\Delta\theta\alpha_T \begin{bmatrix} 1 \\ 1 \\ 0 \end{bmatrix}. \tag{3}$$

The out of plane stress component can be calculated by enforcing the plane strain condition.

The spatial discretization is performed by resorting to the Voronoi tessellation algorithm, able to subdivide a two-dimensional domain into convex polygonal cells starting from a set of nucleation points suitably identified on the domain. First, a regular grid of nucleation points is defined and second, a small random perturbation of point coordinates is applied. The distance between adjacent points is directly related to the mean size of the Voronoi cell. Each Voronoi cell is identified as one element of the finite element discretization.

The hybrid formulation has been implemented by interpolating the stress components over the element domain, through polynomial functions. The stress interpolating functions fulfill *a priori* the indefinite equilibrium equations in absence of body forces.

The solving equations of the finite element model are based on the principle of minimum of the total complementary energy (Π_c). For linear elastic materials the Π_c^e of the eth element is written as follows:

$$\Pi_c^e = \int_{V^e} \left[\frac{1}{2}\boldsymbol{\sigma}^T \mathbf{S}\boldsymbol{\sigma} + \boldsymbol{\sigma}^T\boldsymbol{\theta} \right] \mathrm{d}V - \int_{\partial V_i^e} \mathbf{T}^T\mathbf{u}\,\mathrm{d}s - \int_{\partial V_e^e} \mathbf{T}^T\bar{\mathbf{u}}\,\mathrm{d}s. \tag{4}$$

In this definition, V^e is the element domain, ∂V_i^e is its boundary shared with other adjacent finite elements and ∂V_e^e is the external boundary on which displacements $\bar{\mathbf{u}}$ are prescribed, $\mathbf{u}$ is the vector of unknown displacements.

The vector $\mathbf{T}$, in the integrals over the boundary, collects the surface load components; these are obtained from the equilibrium equation on the boundary : $T_i = \sigma_{ij} n_j$ in which n_j is the component in the direction j of the outward normal defined on the domain boundary.

The polynomial stress interpolation can be written in the following form:

$$\boldsymbol{\sigma} = \mathbf{P}\boldsymbol{\beta} \tag{5}$$

in which $\mathbf{P}$ is matrix of the polynomial terms. The vector $\boldsymbol{\beta}$, defined on the current element, is a vector of constants associated to each relevant term of the polynomial function. In this research, polynomials up to the degree three have been considered.

A discretized form of the total complementary energy for the eth element can be obtained by substituting the stress interpolation (5) into the expression (4):

$$\Pi_c^e = \frac{1}{2}\boldsymbol{\beta}^T \mathbf{H}^e \boldsymbol{\beta} + \boldsymbol{\beta}^T \boldsymbol{\theta}_T^e - \boldsymbol{\beta}^T \mathbf{G}_i^e \mathbf{d}_i - \boldsymbol{\beta}^T \mathbf{G}_e^e \mathbf{d}_e. \tag{6}$$

In (6) the following matrices have been defined:

$$\mathbf{H}^e = \int_{V^e} \mathbf{P}^T \mathbf{S} \mathbf{P}\, \mathrm{d}V; \quad \mathbf{G}_i^e = \int_{\partial V_i^e} \mathbf{P}^T \mathbf{n} \mathbf{L}\, \mathrm{d}S \tag{7}$$

$$\mathbf{G}_e^e = \int_{\partial V_e^e} \mathbf{P}^T \mathbf{n} \mathbf{L}\, \mathrm{d}S; \quad \boldsymbol{\theta}_T^e = \int_{V^e} \mathbf{P}^T \boldsymbol{\theta}\, \mathrm{d}V \tag{8}$$

The displacements vectors $\mathbf{d}_i$ and $\mathbf{d}_e$ collect the displacement unknowns of the problem and the displacement boundary data, respectively. The displacement components along the boundary are linearly interpolated through the interpolation matrix $\mathbf{L}$.

The stationary condition of Π_c^e with respect to the stress parameters $\boldsymbol{\beta}$ yields:

$$\boldsymbol{\beta} = \mathbf{H}^{e-1} \left(\mathbf{G}_i^e \mathbf{d}_i + \mathbf{G}_e^e \mathbf{d}_e - \boldsymbol{\theta}_T^e \right). \tag{9}$$

Substituting (9) into (6), summing up all the contributions over all the elements ($\Pi_c = \sum \Pi_c^e$) and eventually imposing the stationary condition with respect to the unknown displacements $\mathbf{d}_i$, one gets

$$\mathbf{K}\mathbf{d}_i = \mathbf{F} \tag{10}$$

in which the stiffness matrix $\mathbf{K}$ and the right hand side vector $\mathbf{F}$ are:

$$\mathbf{K} = \sum_e \mathbf{G}_i^{eT} \mathbf{H}^{e-1} \mathbf{G}_i^e, \quad \mathbf{F} = -\sum_e \mathbf{G}_i^{eT} \mathbf{H}^{e-1} \mathbf{G}_e^e \mathbf{d}_e + \sum_e \mathbf{G}_i^{eT} \mathbf{H}^{e-1} \boldsymbol{\theta}_T^e. \tag{11}$$

The stiffness matrix and the nodal forces vector are computed in the finite element sense, i.e. the summation over all the elements of the model is carried out through the use of the connectivity relationships between the local degrees of freedom and the model degrees of freedom. This is carried out in the finite element routine that assembles the stiffness matrix $\mathbf{K}$ and the load vector $\mathbf{F}$.

The equilibrium equation (10) has the standard form as that resulting from the solving system of equations in the finite element displacement formulation. This

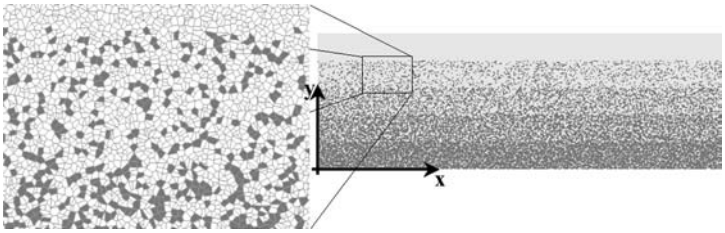

Figure 3. Finite element mesh for the VCFEM model. Details of the polygonal elements are shown in the enlargement, dark and white elements are alumina are zirconia, respectively.

allows for a simple implementation into a commercial finite element code; here the code ABAQUS (Hibbit, Karlsson & Sorensen, Inc.) has been used.

Spatial integration of the matrix **H** has been carried out numerically by subdividing each Voronoi cell in quadrilaterals for identifying the Gauss quadrature points. Spatial integration of the matrix **G** has been carried out analytically by using the symbolic mathematical package MAPLE.

A discussion on the use of the VCFEM formulation and in particular on the stress accuracy for materials exhibiting a microstructure with grains like ceramics and ceramic composites can be found in [23]. Grujcic *et al.* adopt the Voronoi polygonal elements with the purpose to represent the grains of a two phases composite; that is the same approach adopted in this paper.

The finite element mesh of the VCFEM for the plane strain analysis of the laminate under consideration consists of 11 1000 nodes, 52 368 polygonal elements and 20 2807 degrees of freedom; it is shown in Figure 3. A detail of the polygonal finite elements is shown in the enlargement. Dark elements and white elements represent alumina and zirconia, respectively. The left vertical boundary and the top horizontal boundary are stress-free boundaries; the bottom boundary is the symmetry line in the thickness direction, whereas the right vertical boundary is a symmetry boundary in the longitudinal direction.

4. Macroscopic Homogenized Models

4.1. 3D Displacement Based Finite Element Approach

A stress analysis of the laminate, modeled assuming equivalent continuum homogeneous materials, has been carried out with the purpose to compare and validate the results obtained through the microstructural approach.

A three-dimensional standard displacement-based finite element model has been set up. Three planes of symmetry have been identified, and only one eighth of the laminate has been modeled. Therefore the model includes five layers, above the symmetry plane.

The size of the model was chosen such that all free edge effects are negligible far from the free boundary of the model. The size of the model is reported in the Figure 1. The displacement based finite element model consists of 12 3968 nodes and 28 830 quadratic brick elements with twenty nodes. Each lamina is discretized with six layers of elements. In the neighborhood of the free corner, the average element

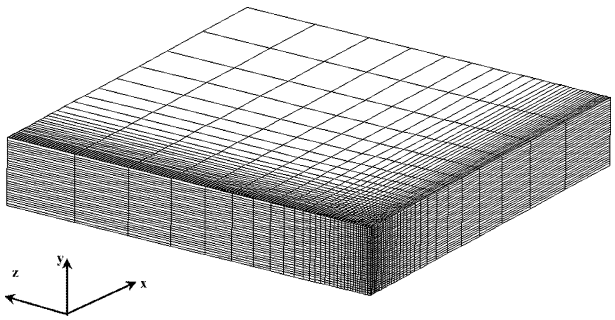

Figure 4. Three-dimensional Finite element mesh of the laminate, only one eighth of the structure is modeled.

size is $1.6\,\mu$m. Displacement boundary conditions are applied along the symmetry planes by constraining the displacement components perpendicular to the plane itself. A uniform temperature change reproducing the cooling process from the sintering temperature to the room temperature is applied ($\Delta\theta = -1600^{\circ}$C). The adopted finite element mesh is reported in Figure 4. To this purpose the commercial finite element code ABAQUS has been used.

4.2. Analytical Approximation of the Residual Stress Field

The residual stress field resulting from the uniform temperature change of a composite laminate can also be estimated through analytical approaches, see for example [16,17].

The one adopted in this paper is based on the assumption of an equilibrium stress distribution with some free parameters. These parameters are obtained through the principle of minimum complementary energy. In particular, the approach presented by Becker *et al.* [16,17] is briefly summarized in the following.

The hypotheses of symmetry of the laminate and of isotropic linear elasticity of each lamina make the analytical approximation rather simple. It is expected that the in-plane shear stress is negligible, therefore it can be assumed that $\sigma_{xz} = 0$; moreover, the stress components σ_{xx} and σ_{xy} are assumed constant with respect to the spatial variable z and the stress components σ_{zz} and σ_{zy} are assumed constant with respect to the spatial variable x. In order to fulfill *a priori* the indefinite equilibrium equations, the stress components are assumed in the following form:

$$\sigma_{xx}(x, y) = [1 - (1 + \phi x)]\mathrm{e}^{-\phi x} g_{xx}(y), \tag{12}$$

$$\sigma_{zz}(y, z) = [1 - (1 + \phi z)]\mathrm{e}^{-\phi z} g_{zz}(y), \tag{13}$$

$$\sigma_{yy}(x, y, z) = \phi^2[1 - \phi x]\mathrm{e}^{-\phi x} g^x_{yy}(y) + \phi^2[1 - \phi z]\mathrm{e}^{-\phi z} g^z_{yy}(y), \tag{14}$$

$$\sigma_{xy}(x, y) = -\phi^2 x\mathrm{e}^{-\phi x} g_{xy}(y), \tag{15}$$

$$\sigma_{zy}(y, z) = -\phi^2 z\mathrm{e}^{-\phi z} g_{zy}(y) \tag{16}$$

with

$$g_{xx}(y) = [E^n_2], \tag{17}$$

$$g_{zz}(y) = [E^n_6], \tag{18}$$

$$g^x_{yy}(y) = [E^n_2 \frac{y^2}{2} + E^n_3 y + E^n_4], \tag{19}$$

$$g^z_{yy}(y) = [E^n_6 \frac{y^2}{2} + E^n_7 y + E^n_8], \tag{20}$$

$$g_{xy} = [E^n_2 y + E^n_3], \tag{21}$$

$$g_{zy} = [E^n_6 y + E^n_7]. \tag{22}$$

The coefficients E^n_i, related to the nth lamina, are constants that are determined through the equilibrium conditions at the interfaces between adjacent laminae and on the external boundary [16].

The assumed stress field (12–16) is dependent on the free parameter ϕ, which accounts for the local stress values close to the free edge, where the solution strongly deviates from the stresses occurring in the inner region (far from the free edge), which can be calculated through the Classical Laminate Theory (CLT).

The parameter ϕ has to be determined through the stationarity condition of the complementary potential energy $\Pi(\phi)$:

$$\Pi(\phi) = \int_V \left[\frac{1}{2} \boldsymbol{\sigma}^T \mathbf{S} \boldsymbol{\sigma} + \boldsymbol{\sigma}^T \boldsymbol{\Delta\theta} \right] \mathrm{d}V \tag{23}$$

with:

$$\boldsymbol{\Delta\theta} = \alpha^H \begin{bmatrix} \Delta\theta \\ \Delta\theta \\ \Delta\theta \\ 0 \\ 0 \\ 0 \end{bmatrix}, \quad \boldsymbol{\sigma} = \begin{bmatrix} \sigma_{xx} \\ \sigma_{yy} \\ \sigma_{zz} \\ \sigma_{xy} \\ \sigma_{xz} \\ \sigma_{yz} \end{bmatrix} \tag{24}$$

The mathematical package MAPLE has been used to obtain the analytical expression (23) and to solve the stationarity condition $\frac{\mathrm{d}\Pi(\phi)}{\mathrm{d}\phi} = 0$.

4.3. Enhancement of the Macroscopic Models

The macroscopic models expounded in the previous two subsections provide an average value of the stresses which are due to the mismatch of the average CTE between laminae. In fact, these models assume a homogeneous isotropic linear elastic material within each lamina. However, the microscopic heterogeneity of the composite induces a deviation of the local stress within the grains of alumina and zirconia, from the average stress predicted by the macroscopic models.

A simple approach, able to estimate the stress within each material component, is discussed in this section. The method is based on the Eshelby tensor approach which defines a composite made of inclusions, having an idealized geometry, embedded in a matrix.

Linear isotropic elasticity with isotropic CTE is assumed for both the alumina and zirconia phases. Since the material grains do not exhibit preferred geometric directions, the ideal case of spherical inclusion is here assumed.

The state of stress within the matrix and the inclusions is given by two distinct contributions: (i) the macroscopic stress owing to the macroscopic spatial mismatch of CTE in the whole laminate ($\boldsymbol{\sigma}^H$); and (ii) the stress concentration, arising within

each phase, owing to the microscopic CTE heterogeneities ($\boldsymbol{\sigma}^{\mu}$). The stresses within the alumina and zirconia phases can be expressed respectively as

$$^{Al_2O_3}\boldsymbol{\sigma} = \boldsymbol{\sigma}^{H} + {}^{Al_2O_3}\boldsymbol{\sigma}^{\mu}, \quad {}^{ZrO_2}\boldsymbol{\sigma} = \boldsymbol{\sigma}^{H} + {}^{ZrO_2}\boldsymbol{\sigma}^{\mu}. \tag{25}$$

Provided the simple geometry of the matrix and of the inclusion in the representative volume element, the stress state due to the temperature change of the composite and to the CTE mismatch between the inclusion and the matrix is hydrostatic, i.e.:

$$^{ZrO_2}\sigma_{ij}^{\mu} = {}^{ZrO_2}\sigma^{\mu}\delta_{ij}, \quad {}^{Al_2O_3}\sigma_{ij}^{\mu} = {}^{Al_2O_3}\sigma^{\mu}\delta_{ij}, \tag{26}$$

being δ_{ij} the Kronecker delta.
Let one introduce two strain fields respectively denoted as *transformation strain* ϵ_{ij}^{t*} and *constrained strain* ϵ_{ij}^{c}. The former accounts for the strain mismatch due to the temperature change of the two materials and has the following form:

$$\epsilon_{ij}^{t*} = \epsilon^{t*}\delta_{ij} = (\alpha_i - \alpha_m)\Delta\theta\delta_{ij}, \tag{27}$$

while the latter is introduced to recover the kinematic compatibility at the interface of the two phases.

The matrix is therefore subjected to ϵ_{ij}^{c} and the inclusion is subjected to $\epsilon_{ij}^{c} - \epsilon_{ij}^{t*}$.

The concept of the equivalent inclusion is now introduced. It defines a fictitious strain field ϵ^{t} such that

$$K_i(\epsilon^{c} - \epsilon^{t*}) = K_m(\epsilon^{c} - \epsilon^{t}), \tag{28}$$

in which K_i and K_m are the bulk moduli of the inclusions and the matrix, respectively.

According to the Eshelby theory one can write a relationship between ϵ^{c} and ϵ^{t} as follows:

$$\epsilon^{c} = (1-f)S_v\epsilon^{t} + f\epsilon^{t} \tag{29}$$

where f is the volume fraction of the inclusions and S_v is the bulk coefficient of the Eshelby tensor defined as:

$$S_v = \frac{1+\nu_m}{3(1-\nu_m)}. \tag{30}$$

Substituting (29) into (28) one gets

$$\epsilon^{t} = \frac{K_i}{(K_i - K_m)(S_v + f - fS_v) + K_m}\epsilon^{t*}. \tag{31}$$

The microscopic stress in the inclusion can be obtained, account taken of (28), as

$$^{i}\sigma^{\mu} = K_m(\epsilon^{c} - \epsilon^{t}) = \frac{K_m K_i(1-f)(S_v - 1)}{(K_i - K_m)(1-f)(S_v - 1) + K_i}\epsilon^{t*}. \tag{32}$$

The average stress in the matrix can be obtained from the equilibrium condition such that

$$^{m}\sigma^{\mu} = {}^{i}\sigma^{\mu}\frac{-f}{(1-f)}. \tag{33}$$

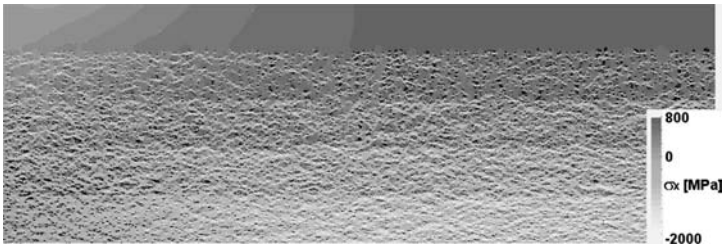

Figure 5. Contour of the longitudinal stress on the symmetry plane ($z = 300\,\mu$m) calculated through the VCFEM.

5. Results

In this section the results of the VCFEM model and of the macroscopic homogeneous models are presented. The results from the macroscopic models have been enhanced through the estimation of the microscopic stress ($\boldsymbol{\sigma}^{\mu}$) as shown in Section (4.3).

The material composition in the five layers was such that a tensile stress develops at the outer layer. The inner layers are characterized by a stress distribution that is strongly affected by the microscopic arrangements of the two phases. Figure 5 shows a gray-scale contour plot of the longitudinal stress component (σ_{xx}) within the laminate. A maximum tensile stress of about 650 MPa is reached in the zirconia layer close to the symmetry plane ($x = 300\,\mu$m). The contour plot shows the free edge effect induced by the stress free boundary condition applied at the free boundary ($x = 0$). The stress values calculated into the inner layers are characterized by fluctuating values due to the presence of zirconia and alumina grains, each exhibiting different elastic properties. In particular, the alumina grains are subjected to a compressive stress while the zirconia grains are subjected to a tensile stress. In the innermost layer (layer 5), a peak compressive stress in the alumina phase of about 2000 MPa has been calculated close to the symmetry plane. In order to have a quantitative comparison between the stress evaluated through the homogenized macroscopic models and that obtained through the VCFEM model, a third order polynomial interpolation of the stress in each material phase of the VCFEM results has been carried out. As a representative example, the Figure 6 shows the interpolation of the longitudinal stress computed in the zirconia grains, in the second layer ($y = 70\,\mu$m).

First, a comparison between the results from the computational microscopic model and those from the homogenized macroscopic models is carried out in the first layer (the outer layer). Since the material in the layer is homogeneous, one has $\sigma^{\mu} = 0$. Figure 7 shows the value of the longitudinal stress (σ_{xx}) along the path $y = 90\,\mu$m, $0 \leqslant x \leqslant 300\mu$m, which is located half layer thickness away from the outer surface ($y = 100\mu$m). In the figure, the stresses calculated through the analytical solution from equations (12–16), the 3D displacement based FEM solution and the VCFEM results are reported. The solution far from the free edge, estimated through the VCFEM approach, was about 700 MPa; while the homogenized models yielded a value of about 650 MPa. This mismatch is due to the plane strain assumption in the computational microscopic model.

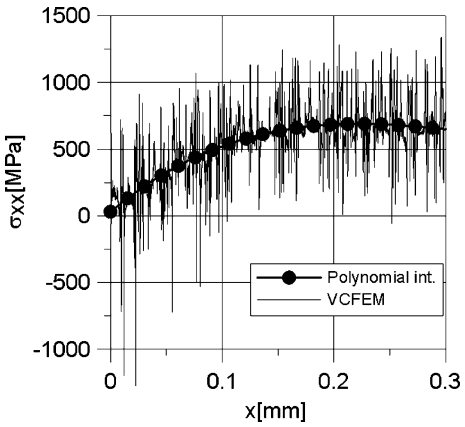

Figure 6. Example of a third order polynomial interpolation of the longitudinal stress in the zirconia phase in the second layer.

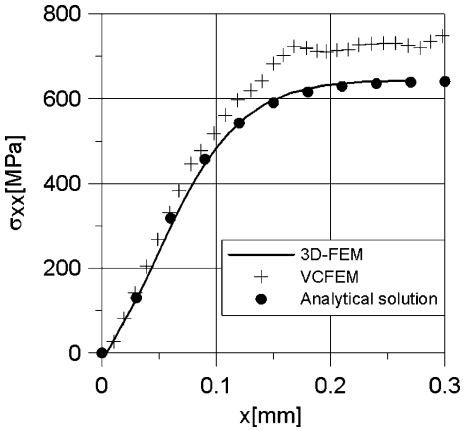

Figure 7. Longitudinal stress in the first layer (pure zirconia).

Figure 8 (right) shows the shear stress component (τ_{xy}) along the same path. The Solid line and the symbols are the 3D-FEM and the VCFEM solutions, respectively; the bullets represents the analytical solution. This component of stress is well estimated by the two finite element approaches, whereas the negative peak value at the free edge (about -15 MPa) has been missed by the analytical approach. The VCFEM results show some fluctuations with respect to the homogenized solution, this was due to the heterogeneities in the lower layers.

Figure 8 (left) shows the transverse stress component (σ_{yy}), computed along the same path. Also in this case the VCFEM model yielded a stress distribution similar to the 3D-FEM, and the fluctuations due to the heterogeneities in the lower layers were also present. The analytical approach missed the negative stress peak (-60 MPa) close to the free edge, similarly to what already observed for the longitudinal stress component.

The comparison between the results of the VCFEM and the homogenized models was also carried out in the layer 2 ($80\%\,ZrO_2/20\%\,Al_2O_3$) along the path $y = 70\,\mu\text{m}, 0 \leqslant x \leqslant 300\,\mu\text{m}$ and in the layer 4 ($40\%\,ZrO_2/60\%\,Al_2O_3$) along the

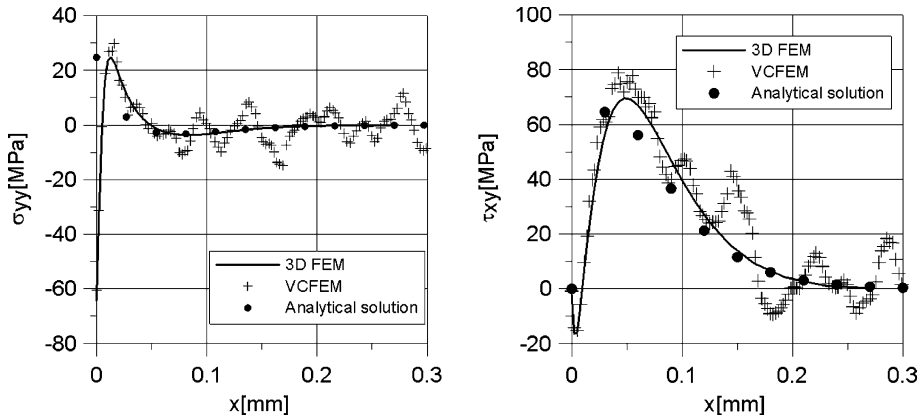

Figure 8. Transverse (left) and shear (right) stress components in the first layer.

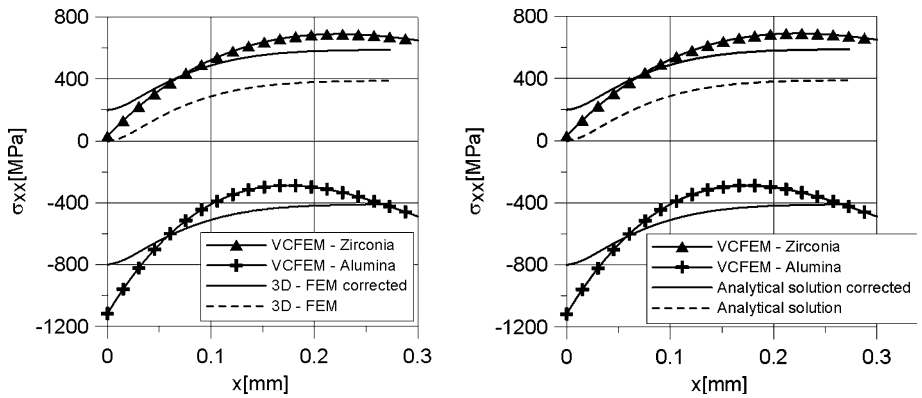

Figure 9. Longitudinal stress in the second layer, comparison between the VCFEM (line with symbols) and the analytical model (solid line) is shown on the left, comparison between the VCFEM (line with symbols) and the 3D-FEM (solid line) is shown on the right. Dashed lines show the average result of the macroscopic model σ^H_{xx}.

path $y = 30\,\mu\text{m}, 0 \leqslant x \leqslant 300\,\mu\text{m}$. In these two layers the microscopic stress σ^μ was calculated according to the equations (32 and 33), in which $f = 0.2$ is the volume fraction of the alumina inclusions for layer 2 and $f = 0.4$ is the volume fraction of the zirconia inclusions for layer 4.

The zirconia matrix in the second layer was subjected to a microscopic hydrostatic tensile stress ${}^{\text{ZrO}_2}\sigma^\mu = 200\,\text{MPa}$ whereas the alumina inclusions were subjected to a microscopic hydrostatic compressive stress ${}^{\text{Al}_2\text{O}_3}\sigma^\mu = -800\,\text{MPa}$. In Figure 9 (right) the longitudinal stress component calculated by means of the analytical homogenized model is reported with a dashed line. The solid lines represent the stresses in the alumina and zirconia phases as obtained from the enhanced macroscopic model. The line with symbols represents the longitudinal stress component, as obtained from the polynomial interpolation of the VCFEM results.

In Figure 9 (left) reports the results in the case of the 3D-FEM homogeneous macroscopic model. The analytical and 3D-FEM approximations provided, in this case, the same response.

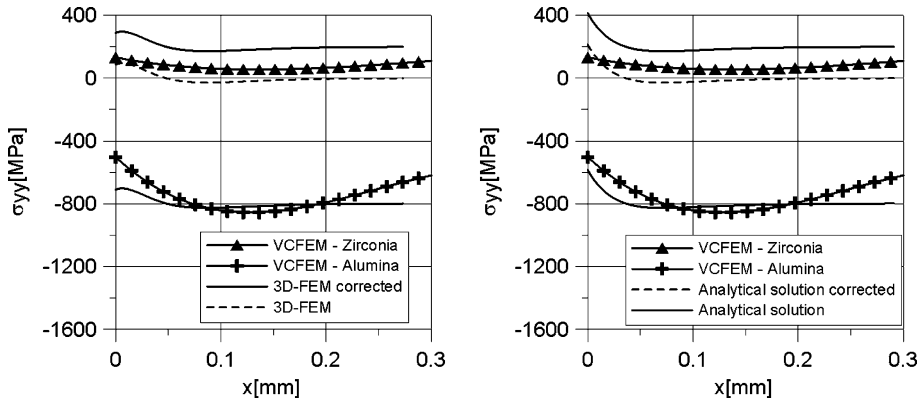

Figure 10. Transverse stress in the second layer, comparison between the VCFEM (line with symbols) and the analytical model (solid line) is shown on the left, comparison between the VCFEM (line with symbols) and the 3D-FEM (solid line) is shown on the right. Dashed lines show the average result of the macroscopic model σ^H_{yy}.

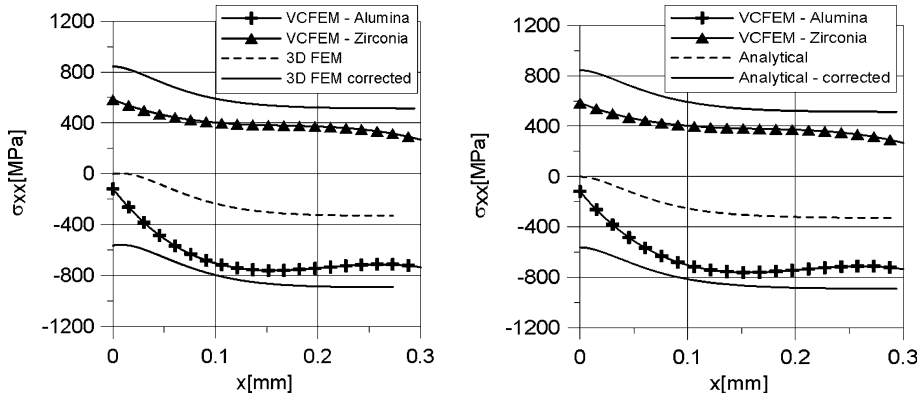

Figure 11. Longitudinal stress in the fourth layer, comparison between the VCFEM (line with symbols) and the analytical model (solid line) is shown on the left, comparison between the VCFEM (line with symbols) and the 3D-FEM (solid line) is shown on the right. Dashed lines show the average result of the macroscopic model σ^H_{xx}.

In Figure 10 the transverse stress components (σ_{yy}) are compared. In this case an appreciable overestimation of the stress in the zirconia phase (in tension) calculated through the enhanced macroscopic models, with respect to that obtained through the VCFEM, can be observed.

The zirconia inclusions in the fourth layer were subjected to a microscopic hydrostatic tensile stress ${}^{ZrO_2}\sigma^{\mu} = 850\,\text{MPa}$, whereas the alumina matrix was subjected to a microscopic hydrostatic compressive stress ${}^{Al_2O_3}\sigma^{\mu} = -550\,\text{MPa}$. Figure 11 (right) shows the comparison between the VCFEM and the analytical model for the longitudinal stress component. Comparison with the 3D-FEM model is shown in Figure 11 (left). Non appreciable difference was observed between the two macroscopic models, whereas the tensile stress in the zirconia phase obtained through the enhanced macroscopic models is overestimated with respect to the VCFEM. A mismatch is also observed in the longitudinal stress of the alumina phase.

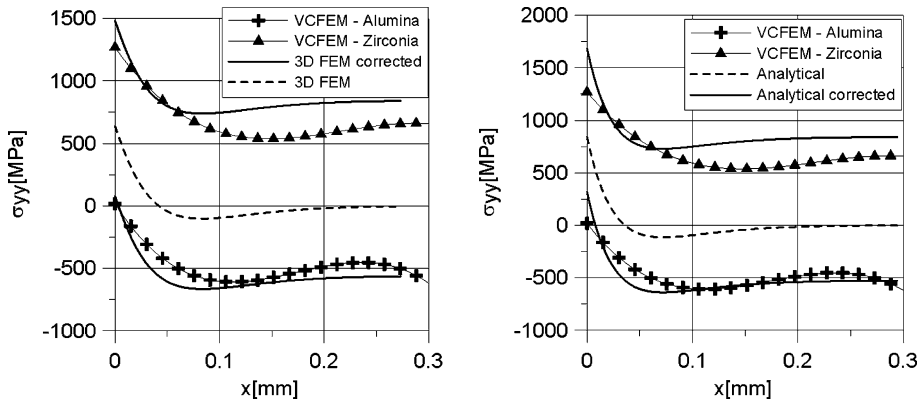

Figure 12. Transverse stress in the fourth layer, comparison between the VCFEM (line with symbols) and the analytical model (solid line) is shown on the left, comparison between the VCFEM (line with symbols) and the 3D-FEM (solid line) is shown on the right. Dashed lines show the average result of the macroscopic model σ_{yy}^{H}.

Similar comparisons for the transverse stress component are reported in the Figure 12. An appreciable mismatch is found between the analytical macroscopic model (Figure 12 – left) and the 3D-FEM macroscopic model (Figure 12 – right) in the evaluation of the tensile stress at the free edge.

6. Discussions and Conclusions

The residual stress field in an alumina/zirconia composite subjected to cooling has been computationally estimated. To this purpose, a micromechanical computational model based on the Voronoi Cell Finite Element Method has been used. Furthermore, a comparison of these results with those obtained through two different homogenized macroscopic models has been provided. The stress concentration induced by the heterogeneities of the ceramic composite has been accounted for, in the macroscopic models, by means of the Eshelby tensor, thus providing an estimate of the residual stress in the zirconia and the alumina phases. The paper focuses on the comparison between the models and does not put emphasis on new phenomena occurring in the ceramic laminate.

The substantial agreement between the two approaches – the VCFEM and the homogenized macroscopic models – has shown that both methods are able to provide a reliable residual stress estimation. In particular, the agreement between the VCFEM and the 3D standard displacement finite element model validates the micromechanical approach.

Advantages and drawbacks of the VCFEM and of the homogenized models can be now delineated.

The microscopic computational model presented in this paper is able to provide the stress state in the alumina and zirconia phases accounting for the geometrical features of the grains and their mutual interactions. As such it is more convenient than the standard displacement-based finite element micromechanical analyses of composites (even if this has not been explicitly proved in this paper). The drawback

of the VCFEM model is the one typical of any micromechanical model, i.e. computational costs actually limit the size of the material domain: only a small size laminate has been considered in this paper; furthermore, reliability of the stress computed at singular points, like grain corners, needs to be enhanced. To this purpose, polynomial interpolation of degree higher than three would be required.

Advantages of the homogenized models are obvious: they are computationally cheaper than any micromechanical analysis and therefore much larger structures may be considered.

The macroscopic models presented in this paper are not able to account for the interaction between the microstructural features (the grains) of the composite, and a simplifying assumption on the shape of the heterogeneities has been used. This assumption might strongly affect the stress concentration factors and justify the mismatch between the stresses in the single phases of the material (Figures 10, 11 and 12).

The major limitations of the microscopic model of the ceramic laminate presented in this paper are: (i) the plane stress assumption and (ii) isotropy of the physical and mechanical properties of the alumina and zirconia grains.

With regards to the first limitation, a quantitative assessment of the error on the longitudinal stress can be estimated on the basis of the theoretical model; whereas the other stress components are not affected by the plane strain assumption.

With regards to the second limitation, anisotropy of the coefficient of thermal expansion may play a role in the estimation of the residual stress at the microscopic level. In [24], Krell *et al.* present an estimation of the residual stresses in single-phase polycrystals. They have found that in homogeneous alumina, anisotropy of the coefficient of thermal expansion causes a residual stress of 148 MPa in the principal crystal direction and -74 MPa in the transversal directions. Lower stresses have been estimated in homogeneous zirconia. These results indicate that in a alumina/zirconia composite, the effect of CTE anisotropy may play a role in the evaluation of the stress in the grains. This residual stress field becomes less important when a composite is considered, indeed higher stresses develop due to the CTE mismatch between alumina and zirconia grains. Moreover, since the principal crystal directions are randomly distributed in the composite, the overall effect of the CTE anisotropy on the macroscopic level vanishes and therefore does not affect substantially the conclusions drawn in this paper. However, further investigations should be addressed in order to study the effect of the CTE anisotropy on local microscopic stress.

Acknowledgements

The financial support from the Politecnico di Milano in the framework of the Project for Young Researchers (Progetto Giovani Ricercatori), year 2000, is gratefully acknowledged.

References

1. Green, D.J., 'Residual stresses in alumina–zirconia laminates', *J. Eur. Ceram. Soc.* **19** (1999) 2511–2517.
2. Sergo, V., Lipkin, M., De Portu, G. and Clarke, D.R., 'Edge stresses in alumina/zirconia laminates', *J. Am. Ceram. Soc.* **80** (1997) 1633–1638.

3. Ho, S., Hillman, C., Lange, F.F. and Suo, Z., 'Surface cracking in layers under biaxial, residual compressive stress', *J. Am. Ceram. Soc.* **78** (1995) 2353–2359.
4. Savoia, M. and Reddy, J.N., 'Three-dimensional thermal analysis of laminated composite plates', *Int. J. Solids Struct.* **32** (1995) 593–608.
5. Rufeng, L. and Xie, Z., 'New finite element method for interlaminar stress analysis of composite laminates at free edge', *Comput. Mech.* (1991) 1025–1030.
6. Gaudenzi, P., Mannini, A. and Carbonaro, R., 'Multi-layer higher-order finite elements for the analysis of free-edge stresses in composite laminates', *Int. J. Numer. Meth. Eng.* **41** (1998) 851–873.
7. Dvorak, G.J. and Zhang, J., 'Transformation field analyses of damage evolution in composite materials', *J. Mech. Phys. Solids* **49** (2001) 2517–2541.
8. Matous, K., 'Damage evolution in particulate composite materials', *Int. J. Solids Struct.* **40** (2003) 1489–1503.
9. Hsueh, C.H. and Becher, P.F., 'Residual thermal stresses in ceramic composites. Part I: with ellipsoidal inclusions', *Mat. Sci. Eng. A – Struct.T* **A212** (1996) 22–28.
10. Biner, S.B., 'Thermo-elastic analisys of functionally graded materials using Voronoi elements', *Mat. Sci. Eng. A-Struct.T* **A315** (2001) 136–146.
11. Schmauder, S. and Weber, U., 'Modelling of functionally graded materials by numerical homogenization', *Arch. Appl. Mech.* **71** (2001) 182–192.
12. Terada, K., Hori, M., Kyoya, T. and Kikuchi, N. 'Simulation of the multi-scale convergence in computational homogenization approaches', *Int. J. Solids Struct.* **37** (2000) 2285–2311.
13. Ghosh, S., Lee, K. and Moorthy, S., 'Multiple scale analisys of hetherogeneous elastic structures using homogenization theory and Vornoi cell finite element method', *Int. J. Solids Struct.* **32** (1995) 27–62.
14. Ghosh, S. and Moorthy, S., 'Elastic-plastic analysis of arbitrary heterogeneous materials with the Voronoi cell finite element method', *Comput. Meth. Appl. Mech. Eng.* **121** (1995) 373–409.
15. Moorthy, S. and Ghosh, S., 'Adaptivity and convergence in the Voronoi cell element model for analyzing heterogeneous materials', *Comput. Meth. Appl. Mech. Eng.*, **185** (2000) 37–74.
16. Becker, W., Jin, P.P. and Lindemann, J., 'The free corner effect in thermally loaded laminates', *Compos. Struct.* **52** (2001) 97–102.
17. Becker, Jr. T.L., Cannon, R.L. and Ritchie R.O., 'An Approximate Method for Residual Stress Calculation in Functionally Graded Materials', *Mech. Mater.* **22** (2000) 85–97.
18. Vena, P., Gastaldi D. and Contro R., 'Mechanical properties of graded ceramic composites for biomedical applications, a computational approach' (in Italian). *Proc. of XVII Italian Congress of Theoretical and Applied Mechanics (AIMETA)*,**CD-rom**,(2003).
19. Chartier, T. and Rouxel, T., 'Tape-cast alumina-zirconia laminates: processing and mechanical properties', *J. Eur. Ceram. Soc.* **17** (1997) 299–308.
20. Hashin, Z. and Shtrikman, S., 'A variational approach to the theory of the elastic behaviour of multiphase materials', *J. Mech. Phys.* **11** (1963) 127–140.
21. Tong, P. and Pian, T.H.H., 'A variational principle and the convergence of a finite element method based on assumed stress distribution', *Int. J. Solids Struct.* **5** (1969) 73–83.
22. Ghosh, S. and Mukhopadhyay, S.N., 'A Material based finite element analysis of heterogeneous media involving dirichlet tessellations'. *Comput. Meth. Appl. Mech. Eng.* **104** (1993) 211–247.
23. Grujicic, M. and Zhang, Y., 'Determination of effective elastic propeties of functionally graded materials using Voronoi cell finite element method', *Mat. Sci. Eng. A – Struct.T* **A251** (1998) 64–76.
24. Krell, A., Teresiak, A. and Schlafer D., 'Grain size dependent residual microstress in submicron Al_2O_3 and ZrO_2', *J. Eur. Ceram. Soc.* **16** (1996) 803–811.